Subcentimeter Precision Ranging System for Moving Targets With a Doppler-Effect-Compensated Ultrasonic Direct Sequence Spread Spectrum

Ishii, Toru

Yoshikawa, Yukiko

Izumi, Shintaro

Kawaguchi, Hiroshi

(Citation)
IEEE Transactions on Instrumentation and Measurement,70:1-8

(Issue Date)
2020-12-29

(Resource Type)
journal article

(Version)
Accepted Manuscript

(URL)
https://hdl.handle.net/20.500.14094/0100477539

Sub-centimeter Precision Ranging System for Moving Targets with a Doppler-Effect-Compensated Ultrasonic Direct Sequence Spread Spectrum

ISHII Toru, Yukiko Yoshikawa, Shintaro Izumi, *Member, IEEE*, and Hiroshi Kawaguchi, *Member, IEEE*

***Abstract*—In this paper, we present a Doppler-effect-compensated ranging system that can be applied to sub-centimeter-precision ultrasonic distance measurement for moving targets using a direct sequence spread spectrum (DSSS). First, the theory of the Doppler compensation technique is explained, and then, the evaluation results obtained using maximum-length-sequence coded ultrasonic signals are discussed. In this study, we employ a 128-bit DSSS code with three wavelengths per bit. The experimental results demonstrate that the proposed system can measure a target accelerating at 9.8 m/s^2 with a speed of up to 2.0 m/s in the range of 0.1–1.6 m, with a standard deviation of less than 5 mm. We also confirmed by simulation that the system can track a target accelerating at 30 m/s^2 with a speed of up to 5.5 m/s in the range of 4–6 m.**

***Index Terms*—Doppler shift, DSSS, M–sequence, Time of arrival, Ultrasound**

I. Introduction

For indoor positioning systems (IPS), in which the radio waves from satellites are severely degraded and for which the global navigation satellite system is not very reliable, a number of systems have been proposed over the past few decades. Nearly a dozen technologies are used in these systems, such as computer vision, magnetic fields, dead reckoning, ultra-wideband, Wi-Fi, and other local radio frequency signals. However, according to Mendoza–Silva et al., achieving a positioning accuracy of less than 10 cm is limited to IPS that use either light or sound [1]. For precise IPS using sound, an ultrasonic direct sequence spread spectrum (DSSS) with maximum-length-sequence (M-sequence) or other similar codes has been proposed [2–14]. DSSS is a technique that increases the signal bandwidth by multiplying a wideband spreading signal, such as an M-sequence, with a data-modulated signal to make the signal more robust against noise or interference [15]. Because of its inherently good characteristics, such as pseudo-random noise, ultrasonic DSSS ranging is advantageous with respect to precision and robustness. However, these characteristics limit the detection of a moving target, and even a slight frequency shift because of the Doppler effect affects the cross correlation of the DSSS code. The correlation coefficients between the received and transmitted signals are poor and sometimes have no peaks. Several studies have attempted to address this issue. Itagaki et al. proposed signal peak tracking with a short reference M-sequence code. For a robot car moving at 0.2 m/s, the estimated mean ranging error was less than 50 mm [8]. Álvarez et al. developed a multifilter bank that could calculate multiple correlation coefficients of the Kasami code with frequency-shifted candidate signals simultaneously [9]. They showed that their system could detect targets moving at a velocity of up to 3 m/s. Widodo et al. directly measured the Doppler shift of a received signal using fast Fourier transform (FFT), and compensated for it accordingly [10]. They successfully performed target tracking on a linear conveyor moving at 0.8 m/s. Other studies estimated the Doppler shift from periodic cycles of the received M-sequence-modulated signal using FFT spectrum analysis [11] [12]. Hirata et al. estimated the Doppler shift by detecting the peak period of the auto-correlation function of the received M-sequence signal. Using the synthetic aperture focusing technique to form the airborne acoustic image from the signals received at different positions, they obtained good experimental results with maximum positioning errors of less than 4 mm for a stainless-steel cylinder moving at 0.24 m/s and 0.36 m/s [13]. However, these methods [11–13] require observation times longer than the interval between signal transmission measurements, which is not suitable for highly accelerating/decelerating target measurements. Albuquerque et al. proposed the introduction of Differential Binary Phase-Shift Keying (DBPSK) modulation and demonstrated that it had better robustness against the Doppler effect than conventional binary phase shift keying (BPSK) [14]. Although DBPSK seems to be promising in terms of precision because of its intrinsic Doppler-free property, it is vulnerable to noise and multiple interferences. Moreover, previous studies [2–14] did not provide the experimental results for a target moving at speeds above 1 m/s, which approximately corresponds to the human walking speed.

To address this issue, a novel Doppler effect compensation technique was presented in our previous study [16], and experimental results showed that it can track a target moving at 2 m/s in the range of 0.1–1.6 m. In this report, further study results of the Doppler compensated ultrasonic DSSS ranging system, in which the dynamic ranging capability was improved using a wideband transducer and a newly developed peak interval detecting algorithm, are presented. The dynamic ranging precision had a standard deviation of less than 5 mm, while the acceleration tracking range in the simulation reached 30 m/s^2. These characteristics are suitable for the potential future applications of IPS to rapidly moving targets, such as drones, pets, or indoor sports athletes in houses, sports gyms, and other common indoor environments.

The corresponding author is ISHII Toru: ishii_toru@cs28.cs.kobe-u.ac.jp. This paper is an extended version of an accepted paper at the IEEE International Instrumentation and Measurement Technology Conference (I2MTC) 2020. This study is based on results obtained from a project commissioned by the New Energy and Industrial Technology Development Organization (NEDO). All the authors are with the Graduate School of Science, Technology and Innovation, Kobe University, Kobe, Japan.

II. Proposed Doppler Shift Compensation

A. Correlation Coefficient Deterioration by Doppler Shift

As reported in previous studies [17] [18], the correlation coefficients in the ultrasonic DSSS range rapidly deteriorate as the relative velocity of the target increases. Fig. 1 shows an example of the cross-correlation between the transmitted and received signals of an M-sequence code when the velocity is sufficiently low such that the main peak Pk_1, at which point the signals coincide between the transmitter and receiver, stands out from others. Here, the cross-correlation was calculated from the convolution of the transmitted and received signals. This means that the largest possible absolute value of the correlation, which determines the vertical axis range of the figure, matches the longer signal length of the two signals when the amplitude of the two signals is normalized to ±1.

As the relative velocity increases, the main peak becomes less prominent because of the Doppler shift. When the velocity exceeds a certain limit, distinguishing the main peak from the others becomes difficult. In our study, the velocity at which $Pk_1 = 2\,Pk_2$ is defined as the "limit velocity," where Pk_1 and Pk_2 are the height of the main peak and the second-highest peak, respectively.

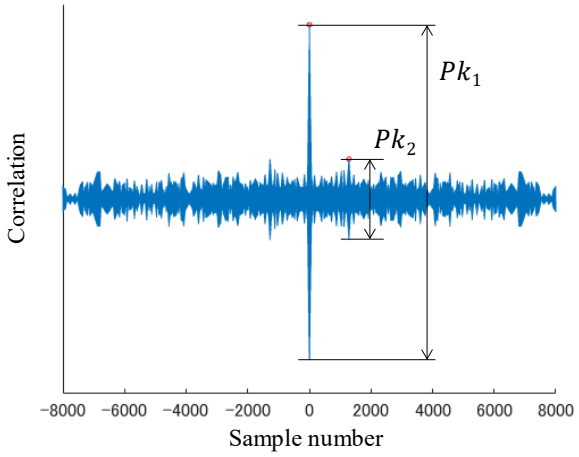

Fig. 1. Cross-correlation between the transmitted and received signals of an M-sequence code. As the relative velocity increases, the main peak Pk_1 becomes less prominent.

Paredes et al. pointed out that the correlation coefficient deterioration in ultrasonic DSSS ranging, caused by Doppler shift, depends on the type of the DSSS code and especially on the code length [18]. Fig. 2 shows the simulation results of the limit velocity of DSSS codes originating from several M-sequences. The horizontal axis L is the length of the transmitted code, which can be defined as $L = N{\cdot}M$, where N is the number of ultrasound carrier wave cycles in one DSSS code bit, and M is the DSSS code length. The error bars in the figure show the minimum and maximum values of the same M and N codes. As shown in the figure, the limit velocity rapidly increases as L decreases.

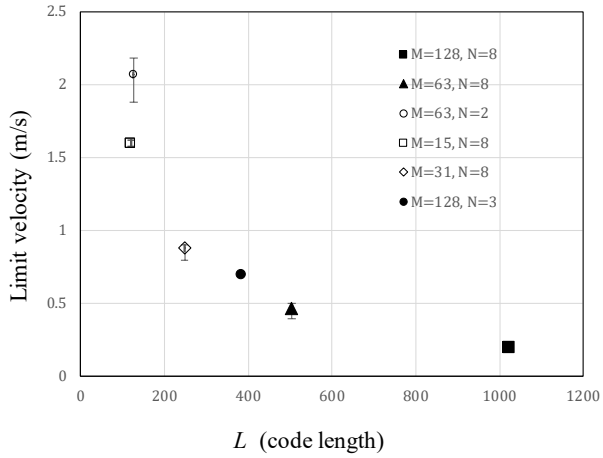

Fig. 2. Simulation results of the limit velocity of M-sequences.

B. Doppler Velocity Estimation

Because the Doppler shift is observed not only in a carrier wave but also in a modulation signal, the Doppler velocity can be estimated from a change in a preknown period of the modulation signal. Fig. 3 shows the principle of the proposed method. In the figure, Tx is a transmitted signal modulated by a certain DSSS code with a bit length of M, i is an index of the code bit, and Tx_a and Tx_b are K-bit long subblocks cut out from different predetermined portions of Tx. Moreover, a and b represent the indices of the top code bit of each portion. Here, ΔT_{ab}, which is a known constant, is the interval between Tx_a and Tx_b, CC_a is the cross correlation between Tx_a and a received signal Rx, CC_b is that between Tx_b and a received signal, and Δt is the interval between the peaks of CC_a and CC_b. The cross correlation CC_i is defined as follows:

$$CC_i(j) = \sum_{k=0}^{K-1} \big(Tx(i+k) \cdot Rx(j+k)\big)\,. \tag{1}$$

Because of the Doppler effect, when the receiver is moving relative to the transmitter, Δt deviates from ΔT_{ab}. Consequently, the Doppler velocity of the receiver is obtained as follows:

$$vd = vs \cdot \left(1 - \frac{\Delta T_{ab}}{\Delta t}\right), \tag{2}$$

where vd is the estimated velocity and vs is the acoustic wave speed in air. K, which is the bit length of Tx_a and Tx_b, should be suitably selected so that it strikes a balance between a sufficiently large limit velocity, which is enabled by the shorter $N{\cdot}K$ to cover the possible Doppler shift; and a sufficient signal noise ratio, which is obtained by the longer K to let CC_a and CC_b peaks remain prominent. Here, N is the same definition as in Fig. 2.

This method is similar to that proposed by Hirata [19], where the Doppler velocity was calculated from the correlation peaks of the two portions of the linear-period-modulation (LPM) signal [19]. However, it is restricted to the LPM signal, whereas our technique can be applied to M-sequences and other DSSS codes.

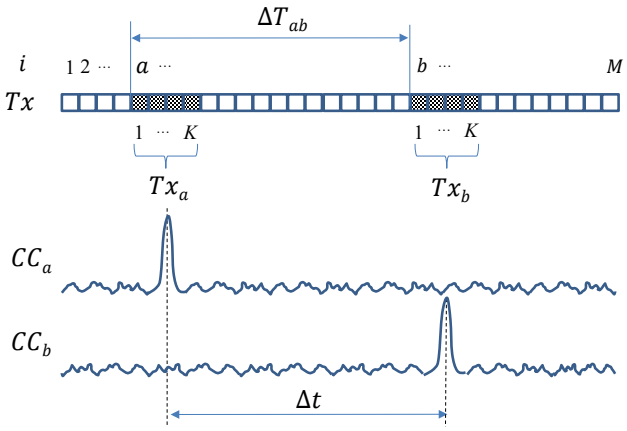

Fig. 3. Principle of the proposed Doppler velocity measurement method.

The newly developed algorithm for detecting the peak interval Δt is shown in Fig. 4, where J is the total number of subblocks, and Δt_j is the peak interval between two adjacent subblocks $\#j$ and $\#j+1$.

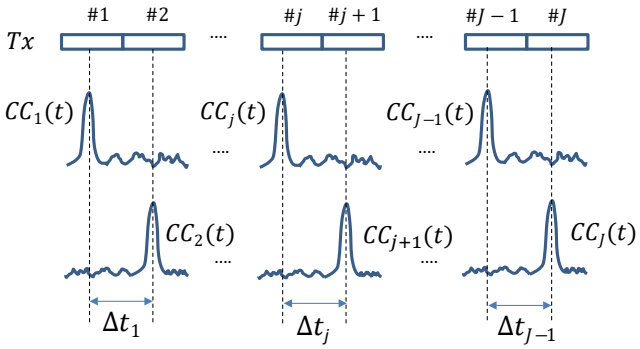

Fig. 4. Peak interval calculation. Δt_i which gives the maximum overlapped accumulation among J-1 candidates is chosen to be the final Δt.

First, $S(i)$, the overlapped accumulation of all the subblocks, is calculated as follows:

$$S(i) = \sum_{j=1}^{J} CC_j(t + (j-1)\cdot \Delta t_i) \quad (3)$$

$$(i = 1..J-1, \text{ where } J = M/K).$$

Then, among the J−1 candidates (Δt_1... Δt_{J-1}), Δt_i, in which i gives the maximum $S(i)$, is chosen to be Δt as the final result.

The present Doppler velocity vd calculated from (2) was not directly used for Doppler compensation. Instead, an estimated velocity v_{est}, given by the following equation, was used as the recurrence relation

$$v_{est} = (1-r)\cdot v_{est_{old}} + r \cdot vd, \quad (4)$$

where r is a smoothing filter coefficient, and v_{est_old} is the old v_{est} used in the previous iteration. The purpose of this filter is to maintain the error between v_{est} and the true Doppler velocity within the limit velocity range shown in Fig. 2, even in an erroneous environment where a single Δt calculation sometimes shows a large error. Here, r should be suitably selected, considering the tradeoff between robustness and a wide dynamic tracking range. In this study, r was preliminarily fixed at 0.7.

C. Doppler Compensation

After the Doppler velocity is known, it can be compensated for by using two methods: modifying either the received or the transmitted signal. The Doppler shift is observed at the receiving end, and the received signal can be modified directly. However, the reference signal, which is the replica of the transmitted signal stored in the receiver, was modified because independent Doppler compensation for each transmitter is preferable in a general multi-transmitter location system. The Doppler compensated reference signal Tx' was obtained by resampling the original reference signal Tx at a sample rate Δt / ΔT_{ab} times that of the original sample rate. Moreover, Tx' was used not only in the cross correlation for the present ranging but also in the Doppler velocity estimation in the next iteration.

III. Evaluation

A. Experimental Environment

The evaluation results are described in this section. Fig. 5 and TABLE I show the experimental setup and list the components, respectively. A 192 kHz high-resolution PC audio interface was used as the signal source. The DSSS-coded wave signal data were stored as a .wav file on the PC. The transmitted signal was output from the DA converter to the ultrasound transducer.

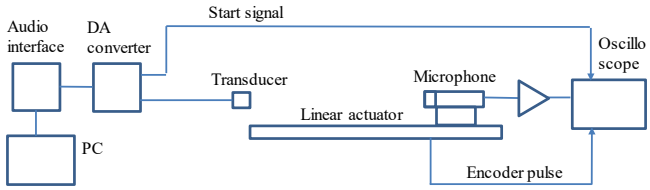

(a) Block diagram

(b) Equipment setup

Fig. 5. Experimental environment

The DA converter's output amplitude was 7.8 Vpp. The center frequency of the transducer was 52 ± 3 kHz. Along with the wave signal, the start signal, which indicates the start time of the wave signal, was synchronously fed to an oscilloscope. The microphone was installed on the stage of the linear actuator, and the signal received through the microphone was amplified by the microphone amp and then fed to the oscilloscope.

TABLE I. KEY COMPONENTS OF THE EXPERIMENT

Component	*Part no.*	*Manufacturer*
Audio Interface	MADI face XT	RME
DA converter	Ferrofish PULSE16MX	Ferrofish
Transducer	480EP900	Pro-Wave
Microphone	TYPE4156N	ACO
Linear actuator	LSA-S8SS-I-100-1620-T2-S	IAI

The oscilloscope simultaneously captured the start signal, received signal, and encoder pulse from the linear actuator; therefore, the raw data for ultrasonic ranging and actuator movement were synchronously stored. The spatial resolution and accuracy of the encoder were 1 mm and ±5 µm, respectively. Both the DSSS coding and Doppler compensation were processed using the software MATLAB. The sampling frequencies of the DA converter and the oscilloscope were 192 kHz and 1.25 MHz, respectively.

B. Static Experiment

For the static evaluation, 100 measurements were taken at 16 fixed positions, from 0.1 to 1.6 m (at every 0.1 m step). TABLE II shows the signal properties of the code used in the experiment. Another bit of "−1" was added at the end of the original 127-bit M-sequence to make the DSSS code length 128. This was done for the convenience of subblock division, which was explained in the Doppler velocity estimation in the previous section.

TABLE II. SIGNAL PROPERTIES FOR STATIC EXPERIMENT

Signal property	*Value*
DSSS code length (M)	128
Carrier wave cycles per bit (N)	3
Code length (L)	384
Subblock length ($N{\cdot}K$)	96
DSSS code	M-sequence
Modulation	BPSK
Carrier wave frequency(fc)	48 kHz
Measurement interval	40 ms

Fig. 6(a) shows the measured distances against the true values. Here, the measured distance is the mean value of the 100 measurements at each point, and the true value is the distance calculated from the encoder pulse. Fig. 6(b) shows the errors in the measurements. The error bar in the figure shows an error range of $\pm 1\sigma$. At 0.5, 0.6, and 0.9 m, relatively large errors were observed, of which the standard deviations were 1.71, 1.24, and 3.62 mm, respectively. At the other distances, the errors were distributed within less than ±0.65 mm, which is on the order of one tenth of the carrier wavelength.

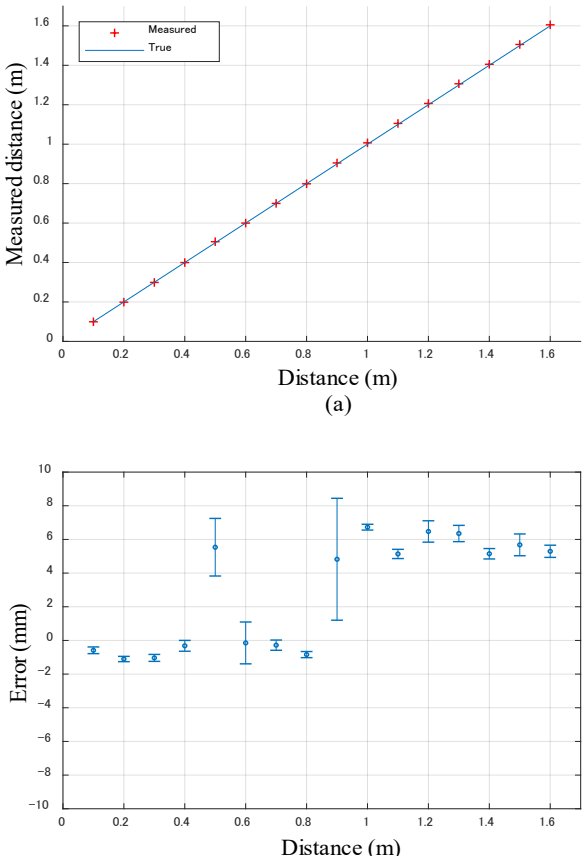

Fig. 6. Static distance measurement.
(a) Measured distance against true value. (b) Ranging error (±1σ).

Fig. 7 shows the magnification of the correlation signals near their maximum peaks at 0.5, 0.6, 0.8, 0.9, and 1.0 m. The plotted lines are the *Tx–Rx* cross correlations in the first measurement at each distance, while the circles in the figure show the maximum peak at all iterations in the measurements. At 0.5, 0.6, and 0.9 m, where the previously mentioned larger errors were observed, either one of the two adjacent peaks, of which the interval is one carrier wavelength, λ (= 7.2 mm), was chosen as the maximum because the height difference between the two was sufficiently small that the maximum peak alternation happened from time to time. The error range at 0.9 m was even larger than that at 0.5 and 0.6 m because the peak alternation occurred more frequently at 0.9 m than at the others. At 0.8 and 1.0 m, the maximum peaks were always fixed to one particular peak in the correlations; however, the maximum peak at 1.0 m stood one λ farther than the true distance. The same results were also observed at a distance from 1.1 to 1.6 m, as shown in Fig. 6(b).

This one-λ farther shift and the above-mentioned maximum peak alternation were caused by multipath interference of the reflected signals from surrounding objects, which distorted the theoretical correlation peak shape. It is possible to mitigate the maximum peak alternation by detecting the envelope peak.

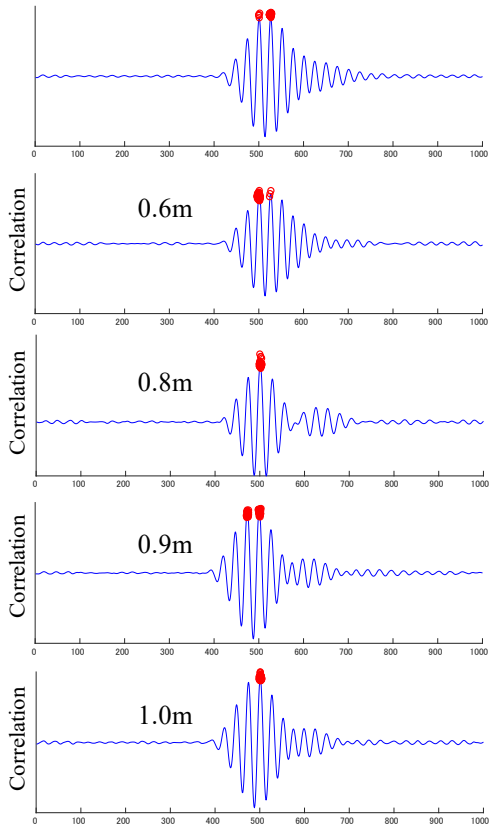

Fig. 7. Correlation signals near the maximum peaks. The maximum peak alternations occurred at 0.5, 0.6 and 0.9m.

Fig. 8 shows the errors in the measurements using the envelope peak detection for the same data as in Fig. 6(b). The error ranges at 0.5, 0.6, and 0.9 m were improved to 0.24, 0.43, and 0.41 mm, respectively, in Fig. 8 from 1.71, 1.24, and 3.62 mm, respectively, in Fig. 6(b).

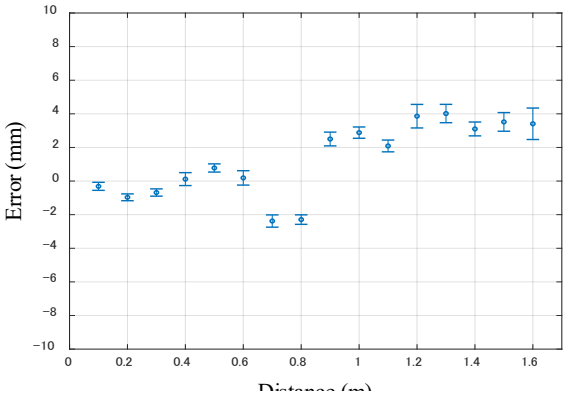

Fig. 8. Ranging error by envelope peak detection (±1σ). The large error bars observed at 0.5, 0.6, and 0.9 m in Fig. 6(b) were improved.

C. *Dynamic Experiment*

For the dynamic experiment, the microphone attached to the stage of the linear actuator was moved back and forth between 0.1 and 1.6 m from the transducer. The signal properties of the codes used in this experiment and the experimental conditions are denoted in TABLE III and TABLE IV, respectively. In addition to the signal listed in TABLE II, another signal from our previous study [16] was also evaluated for comparison. Other properties are the same as those listed in TABLE II.

TABLE III. SIGNAL PROPERTIES FOR DYNAMIC EXPERIMENT

Signal property	***Value***	
DSSS code length (M)	128	
Carrier wave cycles per bit (N)	3	8
Code length (L)	384	1024
Subblock length ($N{\cdot}K$)	96	128
Transducer	480EP900	UTR-1440K-TT-R

TABLE IV. DYNAMIC EXPERIMENTAL CONDITIONS

Distance (m)	0.1–1.6			
Maximum acceleration a_{max} (m/s^2)	2.9	2.9	2.9	9.8
Maximum velocity v_{max} (m/s)	0.5	1.0	1.5	2.0

The measurement results of the short code, $L = 384$, are presented in Fig. 9. The results without compensation and those with the proposed Doppler compensation are shown in Figs. 9(a) and (b), respectively. The ranging errors and the estimated

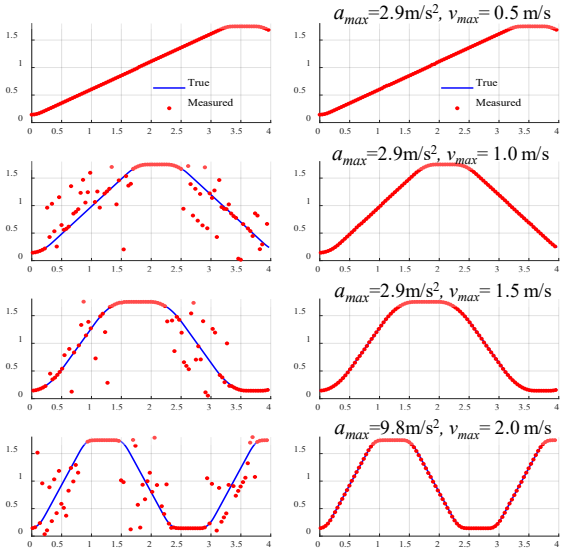

Fig. 9. Dynamic distance measurement with L = 384 (experiment)

(a) Without Doppler compensation

(b) With Doppler compensation

velocity errors in all the Doppler-compensated measurements in one way from 0.11 to 1.59 m, starting at 0 s, in Fig. 9(b) are listed in TABLES V. Here, "Points" indicate the number of measured points in the range, whose errors were calculated. TABLES V indicates that the proposed system could detect the target at all the velocities from 0.5 to 2.0 m/s with a standard deviation (SD) of less than 5 mm in the ranging error, and with one of less than 80 mm/s in the velocity estimation error.

TABLE V. DYNAMIC MEASUREMENT ERRORS ($L = 384$)

a_{max} (m/s^2)	v_{max} (m/s)	Points	Range Error Mean / SD (mm)	Velocity Error Mean / SD (mm/s)
2.9	0.5	75	2.69 / 4.02	25.2 / 45.8
2.9	1.0	40	4.22 / 4.37	−9.6 / 43.4
2.9	1.5	30	5.20 / 4.92	−22.6 / 76.5
9.8	2.0	21	4.54 / 4.47	−22.6 / 77.5

Fig. 10 shows the measurement results of the long code, $L = 1024$. For this code, a more common narrowband transducer UTR-1440K-TT-R was driven at 48 kHz; this was off its center frequency of 40 ± 0.7 kHz, at the cost of power efficiency. The reason behind this tradeoff is to obtain a large limit velocity by making the carrier wave cycles in a code bit as short as 8, which was not attainable at the center frequency. Figs. 10(a) and (b) illustrate the measured distances without and with Doppler compensation, respectively.

As confirmed by the comparison between Figs. 9(a) and 10(a), the longer code is more vulnerable to movement. Even with this long code, however, the proposed compensation technique was effective at all velocities, as shown in Fig. 10(b). The ranging errors and the estimated velocity errors in Fig. 10(b) are listed in TABLE VI. The definitions of the two are the same as those for TABLE V. TABLE VII lists the ranging errors and estimated velocity errors of the best Doppler estimation algorithm from the previous study [16] for the same data as in Fig. 10(b). With the long code, $L = 1024$, TABLES VI and VII indicate that the system could detect the target at all velocities from 0.5 to 2.0 m/s with a standard deviation of less than 7 mm in the ranging error, and with one of less than 100 mm/s in the velocity estimation error, both of which were improved from those in the previous study of less than 11 mm and 160 mm/s, respectively.

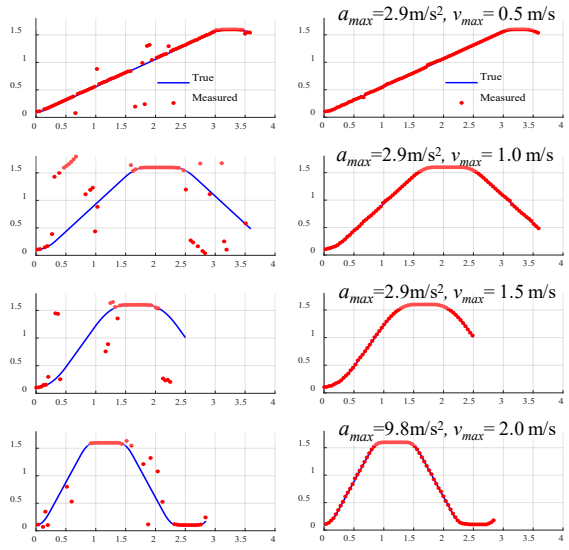

Fig. 10. Dynamic distance measurement with $L = 1024$ (experiment)
(a) Without Doppler compensation
(b) With Doppler compensation

TABLE VI. DYNAMIC MEASUREMENT ERRORS ($L = 1024$)

a_{max} (m/s^2)	v_{max} (m/s)	Points	Range Error Mean / SD (mm)	Velocity Error Mean / SD (mm/s)
2.9	0.5	76	7.53 / 6.52	19.9 / 12.4
2.9	1.0	42	6.18 / 6.29	28.4 / 37.9
2.9	1.5	34	5.29 / 4.53	21.4 / 61.1
9.8	2.0	22	8.60 / 6.37	−24.8 / 95.8

TABLE VII. DYNAMIC MEASUREMENT ERRORS (L =1024) FROM THE PREVIOUS STUDY

a_{max} (m/s^2)	v_{max} (m/s)	Points	Range Error Mean / SD (mm)	Velocity Error Mean / SD (mm/s)
2.9	0.5	76	7.61 / 6.40	3.4 / 58.4
2.9	1.0	42	6.29 / 10.82	-24.2 / 99.2
2.9	1.5	34	4.72 / 4.35	50.7 / 100.2
9.8	2.0	22	10.12 / 8.49	−100.8 / 153.2

D. Simulation

To evaluate the tracking performance of the system for rapid movements beyond the limits of the experimental equipment, a dynamic simulation was carried out. Fig. 11 shows the simulation model. A microphone is attached to one end of an imaginary coil spring, and the other end of the spring is fixed to the wall. A transducer is placed at D away from the microphone when $x = 0$, where x is the deviation from the original relaxed length of the spring. The transducer is in the opposite direction from the microphone to that of the spring. The simulation scenario is as follows: The microphone was once pulled back to $x = -d$ and then released at time $t = 0$, and the microphone was moved back and forth between $D-d$ and $D+d$ from the transducer afterward. The signal properties of the code used in the simulations are the same as those presented in TABLE II.

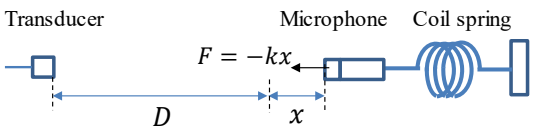

Fig. 11. Simulation model

TABLE VIII presents the initial conditions of the simulation. Here, the maximum acceleration a_{max}, which was originally determined by $a_{max} = kd/m$, where k is the spring constant and m

is the mass of the microphone, is suitably changed for each simulation condition. The a_{max} is applied to the microphone when it is at either end of the stroke ($x = +d, -d$), whereas the maximum velocity v_{max} is observed at the center ($x = 0$).

TABLE VIII. SIMULATION CONDITIONS

Initial distance D (m)	4.8							
Maximum deviation $\pm d$ (m)	±1							
Maximum acceleration a_{max} (m/s^2)	2.5	5	7.5	10	15	20	30	40
Maximum velocity v_{max}(m/s)	1.6	2.2	2.7	3.2	3.9	4.5	5.5	6.3

For the simulation, the seed signal Rx measurement $D = 4.8$ m away from the transducer was first conducted in the same manner as that in the static evaluation, using the same setup as shown in Fig. 5(a), except for the linear actuator. The simulated received signals Rx' at other distances were obtained by resampling Rx at a sample rate that matches the Doppler shift, which is the same as that of the Doppler-compensated transmitted signal Tx' in Section II. Rx' was generated every 40 ms, which corresponds to the measurement interval listed in TABLE II. After the simulated signals Rx' were obtained, ranging signal processing, which was the same calculation sequence as explained in the discussion of the dynamic evaluation, was performed. Fig. 12 presents the simulation results. The results showed that the proposed system could track the movement up to 30 m/s^2 in acceleration.

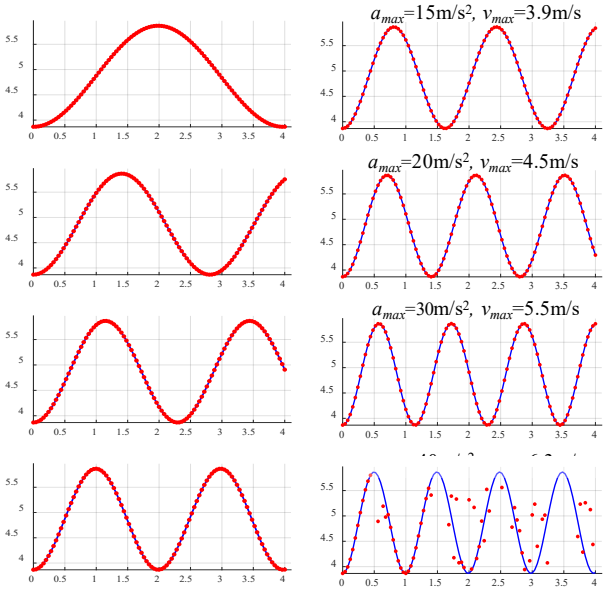

Fig. 12 Dynamic distance measurement (simulation)

IV. CONCLUSION

A Doppler-effect-compensated ranging system for moving targets using ultrasonic DSSS was proposed. The proposed system was evaluated through experiments and simulations. The experimental results show that, with a 128-bit 3-wave-cycle/bit DSSS code, the proposed system can measure a target accelerated at 9.8 m/s^2 and that it reaches up to 2.0 m/s in the range of 0.1–1.6 m, with a standard deviation of less than 5 mm. The simulation results show that the system can track a target accelerated at 30 m/s^2 and can reach up to 5.5 m/s in the range of 4–6 m. These characteristics are suitable for the potential future applications of IPS to rapidly moving targets, such as drones, pets, or indoor sports athletes in houses, sports gyms, and other common indoor environments.

REFERENCES

[1] G.M. Mendoza-Silva, J. Torres-Sospedra, and J. Huerta, "A meta-review of indoor positioning systems," *Sensors*, vol. 19, no. 20, pp. 4507–4551, 2019.

[2] M. Hazas and A. Ward, "A novel broadband ultrasonic location system." in, *Lecture Notes in Computer Science* Intl. Conf. on Ubiquitous Comput. Berlin, Heidelberg: Springer, pp. 264–280, 2002.

[3] M. Hazas and A. Hopper, "Broadband ultrasonic location systems for improved indoor positioning," *IEEE Trans. on Mobile Comput.*, vol. 5, no. 5, pp. 536–547, 2006.

[4] J. C. Prieto, A. R. Jiménez, J. I. Guevara, J. L. Ealo, F. A. Seco, J. O. Roa, and F. X. Ramos, "Subcentimeter-accuracy localization through broadband acoustic transducers." in IEEE Intl. Symp. on Intell. Signal Process. IEEE, 2007, pp. 1–6.

[5] J. C. Prieto, A. R. Jiménez, J. I. Guevara, J. L. Ealo, F. A. Seco, J. O. Roa, and F. X. Ramos., "Performance evaluation of 3D-LOCUS advanced acoustic LPS," *IEEE Trans. Instrum. Meas.*, vol. 58, no. 8, pp. 2385–2395, 2009.

[6] J. R. Gonzalez and C. J. Bleakley, "High-precision robust broadband ultrasonic location and orientation estimation," *IEEE J. Sel. Top. Signal Process.*, vol. 3, no. 5, pp. 832–844, 2009.

[7] C. Sertatıl, M. A. Altınkaya, and K. Raoof, "A novel acoustic indoor localization system employing CDMA," *Digit. Signal Process.*, vol. 22, no. 3, pp. 506–517, 2012.

[8] Y. Itagaki, A. Suzuki, and T. Iyota, "Indoor positioning for moving objects using a hardware device with spread spectrum ultrasonic waves." in Intl. Conf. on Indoor Positioning and Indoor Navig. (IPIN). IEEE, 2012, pp. 1–6.

[9] F. J. Álvarez, Á. Hernández, J. A. Moreno, M. C. Pérez, J. Ureña, and C. De Marziani, "Doppler-tolerant receiver for an ultrasonic LPS based on Kasami sequences," *Sens. Actuators A*, vol. 189, pp. 238–253, 2013.

[10] S. Widodo, S. Tomoo, N. Hayashi, H. Kikuchi, K. Yanagida, Y. Nakatsuchi, Y. Ogawa, and N. Kondo, "Moving object localization using sound-based positioning system with Doppler shift compensation," *Robotics*, vol. 2, no. 2, pp. 36–53, 2013.

[11] S. Hirata and H. Hachiya, "Doppler velocity estimation based on spectral characteristics of M-sequence-modulated signals in ultrasonic measurement for moving objects," *Jpn. J. Appl. Phys.*, vol. 52, no. 7S, 2013, Art. no. 07HC06.

[12] Y. Ikari, S. Hirata, and H. Hachiya, "Ultrasonic position and velocity measurement for a moving object by M-sequence pulse compression using Doppler velocity estimation by spectrum-pattern analysis," *Jpn. J. Appl. Phys.*, vol. 54, no. 7S1, suppl. 1, 2015, Art. no. 07HC14.

[13] S. Hirata, K. Yanamaka, and H. Hachiya, "Evaluation of position and velocity measurement for a moving object by pulse compression using ultrasound coded by preferred-pair M-sequences." in *IEEE International Ultrasonics Symposium (IUS)*. IEEE, 2017, pp. 1–4.

[14] D. F. Albuquerque, J. M. N. Vieira, S. I. Lopes, T. Aguilera, and F. J. Álvarez, "Doppler resilient modulation in a CDMA-based acoustic local

positioning system." in Intl. Conf. on Indoor Positioning and Indoor Navig. (IPIN). IEEE, 2016, pp. 1–8.

[15] A. Goldsmith, "Wireless communications," *Cambridge university press*, 2005.

[16] T. Ishii, Y. Yoshikawa, S. Izumi, and H. Kawaguchi, "Doppler shift compensation technique for ultrasonic DSSS ranging system." in IEEE Int. Instrumentation and Measurement Technology Conf. (I2MTC). IEEE, 2020.

[17] F. J. Alvarez, T. Aguilera, J. A. Paredes, J. Morera, and J. A. Fernández, "Effect of receiver movement on signal detection in an ultrasonic LPS." in *Proc. 2011 Intl. Conf. on Indoor Positioning and Indoor Navigation (IPIN)*. IEEE, 2011, pp. 21–23.

[18] J. A. Paredes, T. Aguilera, F. J. Alvarez, J. Lozano, and J. Morera, "Analysis of Doppler effect on the pulse compression of different codes emitted by an ultrasonic LPS," *Sensors*, vol. 11, no. 11, pp. 10765–10784, 2011.

[19] S. Hirata, M. K. Kurosawa, and T. Katagiri, "An accurate distance measurement by calibration of Doppler-shift for ultrasonic sonar sensing," *J. Acoust. Soc. Am.*, vol. 123, no. 5, pp. 3082–3082, 2008.

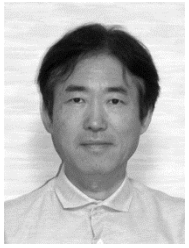

ISHII Toru received a B.Eng. degree in electronic engineering from Kyoto University, Kyoto, Japan, in 1986, and received an MBA degree from Kobe University, Kobe, Japan, in 2013. He joined Minolta, Osaka, Japan, in 1986, where he developed digital imaging devices. He moved to Murata manufacturing, Kyoto, Japan, in 1999, where he was a development manager of automotive radars, communication modules, and sensors. Since 2018, he has been engaged in the research of ultrasound sensing as a postgraduate student at Kobe University.

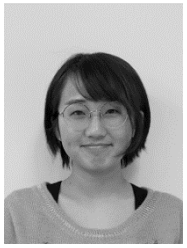

Yukiko Yoshikawa received a B. Eng. degree in Electrical and Electronic Science Engineering from Kobe University, Kobe, Japan in 2019. She is currently in the master's course at Kobe University. Her current research is environmental sensing using an ultrasonic array sensor.

Shintaro Izumi (S'09-M'12) received his B.Eng. and M.Eng. degrees in Computer Science and Systems Engineering from Kobe University, Kobe, Japan, in 2007 and 2008, respectively. He received his Ph.D. degree in Engineering from Kobe University in 2011. He was a JSPS research fellow at Kobe University from 2009 to 2011, an Assistant Professor in the Organization of Advanced Science and Technology at Kobe University from 2011 to 2018, and an Associate Professor at the Institute of Scientific and Industrial Research at Osaka University from 2018 to 2019. Since 2019, he has been an Associate Professor at the Graduate School of System Informatics, Kobe University, Japan. His current research interests include biomedical engineering, biosignal processing, low-power circuit design, and sensor networks.

He has served as a Technical Committee Member for IEEE Biomedical and Life Science Circuits and Systems, as a student activity committee member for the IEEE Kansai Section, and as a Program Committee Member for the IEEE Symposium on Low-Power and High-Speed Chips (COOL Chips). He was a Chair of the IEEE Kansai Section Young Professionals Affinity Group and a recipient of the 2010 IEEE SSCS Japan Chapter Young Researchers Award.

Hiroshi Kawaguchi (M'98) received B.Eng. and M.Eng. degrees in electronic engineering from Chiba University, Chiba, Japan, in 1991 and 1993, respectively, and earned a Ph.D. degree in electronic engineering from The University of Tokyo, Tokyo, Japan, in 2006.

He joined Konami Corporation, Kobe, Japan, in 1993, where he developed arcade entertainment systems. He moved to The Institute of Industrial Science, The University of Tokyo, as a Technical Associate in 1996, and was appointed as a Research Associate in 2003. In 2005, he moved to Kobe University, Kobe, Japan. Since 2007, he has been an Associate Professor with the Department of Information Science at that university. He is also a collaborative researcher at the Institute of Industrial Science, The University of Tokyo. His current research interests include low-voltage SRAM, RF circuits, and ubiquitous sensor networks.

Dr. Kawaguchi was a recipient of the IEEE ISSCC 2004 Takuo Sugano Outstanding Paper Award and the IEEE Kansai Section 2006 Gold Award. He has served as a Design and Implementation of Signal Processing Systems (DISPS) Technical Committee Member for the IEEE Signal Processing Society, as a Program Committee Member for the IEEE Custom Integrated Circuits Conference (CICC) and IEEE Symposium on Low-Power and High-Speed Chips (COOL Chips), and as an Associate Editor of the IEICE Transactions on Fundamentals of Electronics, Communications and Computer Sciences and IPSJ Transactions on System LSI Design Methodology (TSLDM). He is a member of the IEEE, ACM, IEICE, and IPSJ.